Numerical Treatment for the Second Law Analysis in Hydromagnetic Peristaltic Nanomaterial Rheology: Endoscopy Applications

Muhammad Awais
COMSATS University Islamabad
Muhammad Shoaib
COMSATS University Islamabad
Muhammad Asif Zahoor Raja
National Yunlin University of Science and Technology
Saba Arif
COMSATS University Islamabad
Muhammad Yousaf Malik
King Khalid University
Kottakkaran Sooppy Nisar (n.sooppy@psau.edu.sa)
Prince Sattam Bin Abdulaziz University

Research Article

Keywords: Peristaltic flow, Couple stress fluid, Magnetic field, Entropy generation, Mixed convection, Endoscope, Heat transfer

Posted Date: July 19th, 2021

DOI: https://doi.org/10.21203/rs.3.rs-709319/v1

Numerical Treatment for the Second Law Analysis in Hydromagnetic Peristaltic Nanomaterial Rheology: Endoscopy Applications

Muhammad Awais[1, a], Muhammad Shoaib[1, b], Muhammad Asif Zahoor Raja[2, c] , Saba Arif[1, d] , Muhammad Yousaf Malik[3, e], Kottakkaran Sooppy Nisar[4,*]

[1]Department of Mathematics, COMSATS University Islamabad, Attock Campus, Attock 43600, Pakistan

awais@ciit-attock.edu.pk[a]; dr.shoaib@cuiatk.edu.pk[c] ; sabaarif7783@gmail.com[d]

[2]Future Technology Research Center, National Yunlin University of Science and Technology, 123 University Road, Section 3, Douliou, Yunlin 64002, Taiwan, R.O.C.

rajamaz@yuntechedu.tw[b]

[3]Department of Mathematics, College of Sciences, King Khalid University, Abha 61413, Saudi Arabia;

drmymalik@qau.edu.pk[e]

Department of Mathematics, College of Arts and Sciences, Wadi Aldawaser, 11991, Prince Sattam bin Abdulaziz University, Saudi Arabia; n.sooppy@psau.edu.sa

*Corresponding author

Abstract: In current study, analysis is presented for peristaltic motion of applied magnetic field and entropy generation within couple stress (Cu/H_2O) nanofluid through an endoscope. An endoscope contains two coaxial cylindrical tubes in which the internal tube is nonflexible while the external tube has sinusoidal wave passing through the boundary. Influences of mixed convection along with applied magnetic field are encountered as well. Formulated governing model is fabricated introducing long wavelength and creeping Stokesian flow approximation which are then analyzed numerically by utilizing Adams Bashforth method. For a physical insight, results are demonstrated to examine the behaviors of flow profiles and entropy generation number for emerging flow parameters with the help of graphs, bar-charts and tables.

Keywords: Peristaltic flow, Couple stress fluid, Magnetic field, Entropy generation, Mixed convection, Endoscope, Heat transfer.

1: Introduction

Researchers have gained much attention in the study of non-Newtonian fluid behaviors owing to its novel applications in physiology, industry and technological processes. Non Newtonian fluids possess nonlinear relationship among the rate of strain and shear stresses. Among the theories of non-Newtonian fluids, couple stress fluid theory is important one which is further a subclass of polar fluid theories, introduced by Stokes. Constitutive relation that describes the behavior of couple stress fluids encounters couple stresses along with classical Cauchy stress. Moreover, it is oversimplification of the conventional theory of Newtonian fluids which validates polar effects. Such fluids include biological fluids, cosmetics, slurries and dairy wastes etc. Characteristically, Devakar and Iyengar [1] has been investigated flow dynamics of couple stress fluid configured inside two parallel plates. Geometries of the cylindrical pipes with slip wall conditions and analysis of couple stress fluid transport between the parallel surfaces have been obtained by Devakar et al. [2] and [3]. Srivastava [4] analyzed consequences of axially symmetric mild stenosis for blood transport presuming blood as couple stress fluid. In order to inspect the performance of rheological complex fluids, investigations pertaining couple stress fluid are incredibly constructive [5-10].

Furthermore, since several realistic fluids serve as couple stress fluids and owing to their remarkable applications in heat transfer fields, thermal characteristics can be amplified by suspending particles having nanometer size called nanoparticles pioneered by Choi [11]. For instance, Khan et al. [12] have been investigated couple stress nanofluid flow through an oscillatory stretching sheet presuming the impacts of mixed convection with heat generation/ absorption. Some remarkable applications regarding couple stress nanofluids are [13-16].

Peristaltic motion has extensive applications in engineering processes, physiology and industry. In many biological systems, peristalsis has become one of the major apparatus for the fluid transport, initially investigated by Engelman [17]. Recently, Hayat et al. [18] have been investigated impacts of convective conditions and nanoparticles on the peristaltic transport, simultaneously. Moreover, endoscope has many clinical applications. For medical recognition, the endoscope/annulus has important effects on the peristaltic flow. In cancer therapy, for desirable tissues removal; heat transfer is very extensively applicable. For instance, heat transfer in peristaltic flow through a vertical porous annulus has been presented by Vajravela et al. [19]. The closed form solution of a nanofluid for the peristalsis in an annular section has been presented by Shahzadi and Nadeem [20]. Entropy generation analysis in peristalsis of nanofluids due to complex flow structures has

motivated the researchers. Entropy production in peristaltically occurred nanofluid flow has been analyzed by Hayat et al. [21]. The generation of entropy for couple stress fluid has been studied by Jangli et al [22]. Further studies for fluid flows with entropy generation analysis can be seen in references [23-25].

Magneto hydrodynamic explains the magnetic aspects of electrically conducting fluid and have numerous important usages in controlling the velocity of fluids by implementing magnetic field effects. Recently, Awan et al. [26] inspected numerically an unsteady hydro-magnetic nanofluid flow and heat transfer through channel. Simulation of computational fluid dynamics for suspension of nanoparticles in MHD liquid has been analyzed by Nawaz et al. [27]. Some ongoing researches can be seen through the references [28-30]. By utilizing the knowledge of pre-mentioned literature, the aim of current research is to solve numerically the flow and heat exchange for couple stress nanofluid with entropy generation in existence of applied magnetic field and viscous dissipation. The influences of emerging flow parameters are studied and results are demonstrated through graphs.

2: Problem development and governing model

Assume the peristaltic motion of incompressible couple stress (Cu/water) nanofluids conducted in an endoscope. Along the tube wall, sinusoidal wave is transmitting with a uniform speed c. Cylindrical coordinate structure (R, Z) is preferred where Z-axis is passing through the central line and R indicates the radial direction as depicted in **Fig. 1a**. For a_1 and a_2 being radii of internal and external tubes in endoscope, wave forms in fixed frame are written as [31, 32]:

$$r_1 = a_1, \tag{1}$$

$$r_2 = a_2 + b\sin\frac{2\pi}{\lambda}\left(Z - ct\right). \tag{2}$$

In which λ is the wavelength, b is the amplitude of wave and t represents time of travelling wave. Moreover, T_1 and T_0 denote temperature of internal and external cylinders, accordingly.

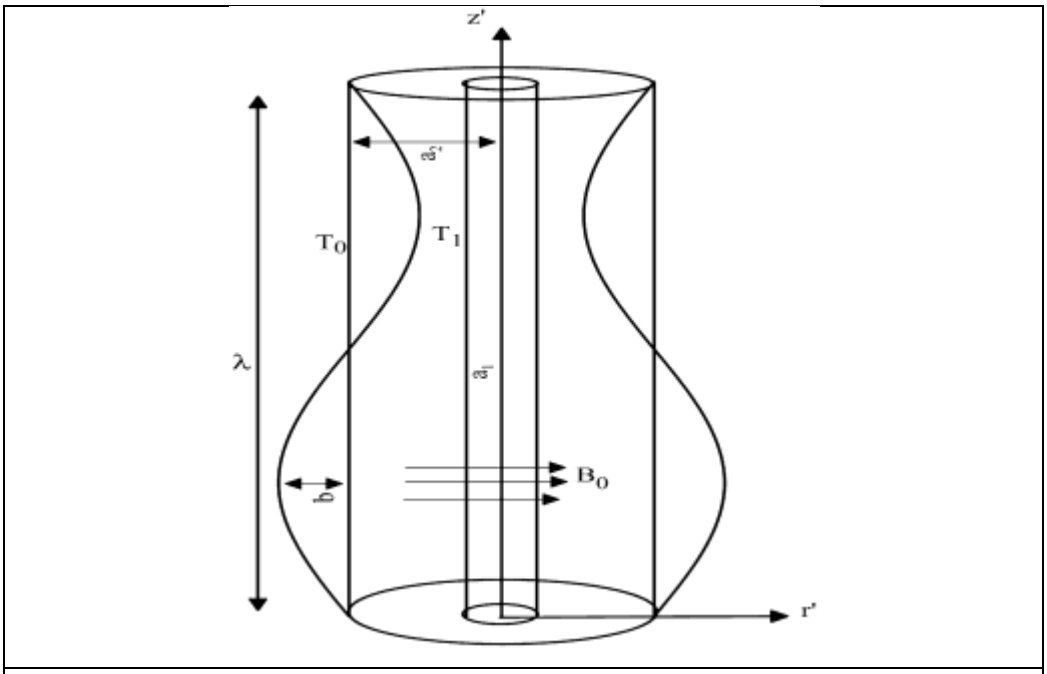

Fig. 1a: Geometrical representation of flow problem.

The constitutive equations governing couple stress tensor M and stress tensor τ are formulated as [7, 8, 32]:

$$\tau = \left(-P + \lambda_1 \nabla . \bar{q}\right) I + \mu\left[\nabla \bar{q} + (\nabla \bar{q})^T\right] + \frac{1}{2} I \times \left(\nabla . M + \rho C\right), \tag{3}$$

$$M = mI + 2\eta \nabla\left(\nabla \times \bar{q}\right) + 2\eta'\left(\nabla\left(\nabla \times \bar{q}\right)\right)^T. \tag{4}$$

In which, m denotes the $\frac{1}{3}$ trace of M , μ and λ_1 express coefficients of viscosity, C indicates vector of body couple while η and η' stand for coefficients of couple stress viscosity. The inequalities constraints for these material constants are given as:

$$\mu \geq 0, \quad 3\lambda_1 + 2\mu \geq 0, \quad \eta \geq 0, \quad \left|\eta'\right| \leq \eta. \tag{5}$$

In view of the above relations (3) and (4), the simplified equations in fixed frame of reference are [36]:

$$\frac{\partial U}{\partial R} + \frac{U}{R} + \frac{\partial W}{\partial Z} = 0, \tag{6}$$

$$\rho_{nf}\left(\frac{\partial U}{\partial t} + U\frac{\partial U}{\partial R} + W\frac{\partial U}{\partial Z}\right) = -\frac{\partial P}{\partial R} + \mu_{nf}\left(\frac{\partial^2 U}{\partial R^2} + \frac{1}{R}\frac{\partial U}{\partial R} - \frac{U}{R^2} + \frac{\partial^2 U}{\partial Z^2}\right) - \eta\left(\frac{\partial^4 U}{\partial R^4} + 2\frac{\partial^4 U}{\partial R^2 \partial Z^2}\right.$$

$$+\frac{\partial^4 U}{\partial Z^4}+\frac{2}{R}\frac{\partial^3 U}{\partial R^3}+\frac{2}{R}\frac{\partial^3 U}{\partial R\partial Z^2}-\frac{3}{R^2}\frac{\partial^2 U}{\partial R^2}-\frac{2}{R^2}\frac{\partial^2 U}{\partial Z^2}+\frac{3}{R^3}\frac{\partial U}{\partial R}-\frac{3}{R^4}U\Bigg), \tag{7}$$

$$\rho_{nf}\left(\frac{\partial W}{\partial t}+U\frac{\partial W}{\partial R}+W\frac{\partial W}{\partial Z}\right)=-\frac{\partial P}{\partial Z}+\mu_{nf}\left(\frac{\partial^2 W}{\partial R^2}+\frac{1}{R}\frac{\partial W}{\partial R}+\frac{\partial^2 W}{\partial Z^2}\right)-\eta\Bigg(\frac{\partial^4 W}{\partial R^4}+\frac{\partial^4 W}{\partial R^2\partial Z^2}$$

$$+\frac{\partial^4 W}{\partial Z^4}+\frac{2}{R}\frac{\partial^3 W}{\partial R^3}+\frac{2}{R}\frac{\partial^3 W}{\partial R\partial Z^2}-\frac{1}{R^2}\frac{\partial^2 U}{\partial R^2}+\frac{1}{R^3}\frac{\partial W}{\partial R}\Bigg)+g\left(\rho\beta_T\right)_{nf}\left(\mathrm{T}-\mathrm{T}_0\right)-\sigma_{nf}B_0{}^2W, \tag{8}$$

$$\left(\rho c_p\right)_{nf}\left(\frac{\partial T}{\partial t}+U\frac{\partial T}{\partial R}+W\frac{\partial T}{\partial Z}\right)=k^*{}_{nf}\left(\frac{\partial^2 T}{\partial R^2}+\frac{1}{R}\frac{\partial T}{\partial R}+\frac{\partial^2 T}{\partial Z^2}\right)+Q_0+\Phi. \tag{9}$$

In aforementioned model, *P* and *T* represent temperature and pressure of fluid whereas *U* and *W* express the *R* and *Z* components of velocity, respectively. Further, g expresses gravitational acceleration, B_0 indicates intensity of external applied magnetic field, Φ denotes dissipation function and Q_0 is heat generation parameter.

In the laboratory frame (*R, Z*), flow is unsteady. In order to obtain a steady flow, transformations of quantities from the laboratory structure (*R, Z*) to the wave structure (r, z) are [7, 32]:

$$r=R,\quad \mathrm{z}=\mathrm{Z}-\mathrm{c}t,\quad \mathrm{u}=\mathrm{U},\quad \mathrm{w}=\mathrm{W}-\mathrm{c},\quad \mathrm{p}=\mathrm{P}. \tag{10}$$

Where, *u* and *v* denote the velocity components in the wave frame (*r, z*). Equations (5)-(8) yields:

$$\frac{\partial u}{\partial r}+\frac{u}{r}+\frac{\partial w}{\partial z}=0, \tag{11}$$

$$A^*\left(u\frac{\partial u}{\partial r}+\left(w+c\right)\frac{\partial u}{\partial z}\right)=-\frac{1}{\rho_f}\frac{\partial p}{\partial r}+\frac{\mu_f}{\rho_f}\frac{1}{A_1}\left(\frac{\partial^2 u}{\partial r^2}+\frac{1}{r}\frac{\partial u}{\partial r}-\frac{u}{r^2}+\frac{\partial^2 u}{\partial z^2}\right)$$
$$-\eta\left(\frac{\partial^4 u}{\partial r^4}+2\frac{\partial^4 u}{\partial r^2\partial z^2}+\frac{\partial^4 u}{\partial z^4}+\frac{2}{r}\frac{\partial^3 u}{\partial r^3}+\frac{2}{r}\frac{\partial^3 u}{\partial r\partial z^2}-\frac{3}{r^2}\frac{\partial^2 u}{\partial r^2}-\frac{2}{r^2}\frac{\partial^2 u}{\partial z^2}+\frac{3}{r^3}\frac{\partial u}{\partial r}-\frac{3}{r^4}u\right), \tag{12}$$

$$A^*\left(u\frac{\partial w}{\partial r}+\left(w+c\right)\frac{\partial w}{\partial z}\right)=-\frac{1}{\rho_f}\frac{\partial p}{\partial z}+\frac{\mu_f}{\rho_f}\frac{1}{A_1}\left(\frac{\partial^2 w}{\partial r^2}+\frac{1}{r}\frac{\partial w}{\partial r}+\frac{\partial^2 w}{\partial z^2}\right)$$
$$-\eta\left(\frac{\partial^4 w}{\partial r^4}+\frac{\partial^4 w}{\partial r^2\partial z^2}+\frac{\partial^4 w}{\partial z^4}+\frac{2}{r}\frac{\partial^3 w}{\partial r^3}+\frac{2}{r}\frac{\partial^3 w}{\partial r\partial z^2}-\frac{1}{r^2}\frac{\partial^2 u}{\partial r^2}+\frac{1}{r^3}\frac{\partial w}{\partial r}\right) \tag{13}$$
$$+\mathrm{g}\left(\rho\beta_T\right)_f A_2\left(T-T_0\right)+\sigma_f A_4 B_0{}^2\left(w+c\right),$$

$$A_5\left(u\frac{\partial T}{\partial r}+\left(w+c\right)\frac{\partial T}{\partial z}\right)=\frac{k_f}{\left(\rho c_p\right)_f}A_3\left(\frac{\partial^2 T}{\partial r^2}+\frac{1}{r}\frac{\partial T}{\partial r}+\frac{\partial^2 T}{\partial z^2}\right)+\frac{Q_0}{\left(\rho c_p\right)_f}+\Phi. \tag{14}$$

Where, constants involved in the above model are:

$$A^{*}=\left(1-\phi\right)+\phi\frac{\rho_s}{\rho_f},\ \ \mathrm{A}_1=\left(1-\phi\right)^{2.5},\ A_2=\left(1\text{-}\phi\right)+\phi\frac{\left(\rho\beta_T\right)_s}{\left(\rho\beta_T\right)_f},$$

$$A_3=\frac{k_s+2k_f-2\phi\left(k_f-k_s\right)}{k_s+2k_f+2\phi\left(k_f-k_s\right)},\ A_4=\left(1-\phi\right)+\phi\frac{\sigma_s}{\sigma_f},\ A_5=\left(1-\phi\right)+\phi\frac{\left(\rho c_p\right)_s}{\left(\rho c_p\right)_f}. \tag{15}$$

Where ϕ is volume fraction of nanoparticles whereas μ_{nf}, ρ_{nf}, $(\beta_T)_{nf}$, σ_{nf} and k^{*}_{nf} symbolizes the dynamic viscosity, density, thermal expansion coefficient, electric conductivity and thermal conductivity of nanofluid. Moreover, μ_{nf}, ρ_s, $(\beta_T)_s$, σ_s and k_s are dynamic viscosity, density, thermal expansion coefficient, electric conductivity and thermal conductivity of nanoparticles while μ_f, ρ_f, k_f, σ_f and $(\beta_T)_f$ represents base liquid viscosity, density, thermal conductivity, electric conductivity and thermal expansion coefficient, respectively. Now, introducing dimensionless variables as [35]:

$$\bar{r}=\frac{r}{a_2},\ \ \bar{r_1}=\frac{r_1}{a_2}=c<1,\ \ \bar{r_2}=\frac{r_2}{a_2}=1+\phi\sin(2\pi z),\ \bar{u}=\frac{\lambda}{a_2c}u,\ \ \bar{z}=\frac{z}{\lambda},\ \phi=\frac{b}{a_2}<1,$$

$$\bar{w}=\frac{w}{c},\ \ \delta=\frac{a_2}{\lambda},\ \ \bar{t}=\frac{ct}{\lambda},\ \ \mathrm{Re}=\frac{\rho_f c a_2}{\mu_f},\ \ \upsilon=\frac{\mu_f}{\rho_f},Gr=\frac{\rho_f g\left(\beta_T\right)_f {a_2}^2\left(T_1-T_0\right)}{\mu_f c},$$

$$\bar{p}=\frac{{a_2}^2}{\lambda\mu_f c}p,\ \ \beta=\frac{Q_0{a_2}^2}{k_f\left(T_1-T_0\right)},\ \ \theta=\frac{\left(T-T_0\right)}{\left(T_1-T_0\right)},\ \ \mathrm{y}=\sqrt{\frac{\eta}{\mu_f{a_2}^2}},\ \mathrm{Pr}=\frac{\mu_f\left(c_p\right)_f}{k_f},$$

$$\bar{\psi}=\frac{\psi}{\mathrm{a_2c}},\ \bar{\mathrm{u}}=-\frac{\delta}{\bar{\mathrm{r}}}\frac{\partial\dot{\psi}}{\partial\bar{\mathrm{z}}},\ \bar{\mathrm{w}}=\frac{1}{\bar{\mathrm{r}}}\frac{\partial\bar{\psi}}{\partial\bar{\mathrm{r}}},\ \ \mathrm{Ec}=\frac{c^2}{\left(c_p\right)_f\left(T_1-T_0\right)},\ \ \mathrm{M}^2=\frac{\sigma_f{B_0}^2{a_2}^2}{\mu_f}. \tag{16}$$

With the help of long wavelength and creeping flow approximations equation (11) is identically fulfilled while equations (12)-(14) reduces to the following expressions:

$$\frac{\partial p}{\partial r}=0, \tag{17}$$

$$y^2\left(\frac{\partial^2}{\partial r^2}+\frac{1}{r}\frac{\partial}{\partial r}\right)^2\left(\frac{1}{r}\frac{\partial\psi}{\partial r}\right)-\frac{1}{A_1}\left(\frac{\partial^2}{\partial r^2}+\frac{1}{r}\frac{\partial}{\partial r}\right)\left(\frac{1}{r}\frac{\partial\psi}{\partial r}\right)=-\frac{1}{A_1}\frac{\partial p}{\partial z}+A_2Gr\theta-A_4M^2\left(\frac{1}{r}\frac{\partial\psi}{\partial r}+1\right), \tag{18}$$

By differentiating equation (18) with respect to *r*, we get the following expression:

$$y^2 \frac{\partial}{\partial r}\left(\frac{\partial^2}{\partial r^2}+\frac{1}{r}\frac{\partial}{\partial r}\right)^2\left(\frac{1}{r}\frac{\partial \psi}{\partial r}\right)-\frac{1}{A_1}\frac{\partial}{\partial r}\left(\frac{\partial^2}{\partial r^2}+\frac{1}{r}\frac{\partial}{\partial r}\right)\left(\frac{1}{r}\frac{\partial \psi}{\partial r}\right)-A_2 Gr\frac{\partial \theta}{\partial r}+$$
$$A_4 M^2 \frac{\partial}{\partial r}\left(\frac{1}{r}\frac{\partial \psi}{\partial r}+1\right)=0, \tag{19}$$

$$A_3\left(\frac{\partial^2 \theta}{\partial r^2}+\frac{1}{r}\frac{\partial \theta}{\partial r}\right)+\beta+A_1 Ec\,\mathrm{Pr}\left(\frac{-1}{r^2}\frac{\partial \psi}{\partial r}+\frac{1}{r}\frac{\partial^2 \psi}{\partial r^2}\right)^2=0. \tag{20}$$

Bar notation is ignored. Here, *Re, Ec*, *Pr* and *Gr* indicates Reynolds number, Eckert number, Prandtl number and thermal Grashof number whereas δ expresses wave number and θ is the dimensionless temperature. Moreover, ψ is stream function for which components of velocity are derived as:

$$u=\frac{1}{r}\frac{\partial \psi}{\partial r}, v=-\frac{\delta}{r}\frac{\partial \psi}{\partial z}.$$

The dimensionless boundary conditions are:

$$\frac{1}{r}\frac{\partial \psi}{\partial r}=-1,\ \frac{\partial^2}{\partial r^2}\left(\frac{1}{r}\frac{\partial \psi}{\partial r}\right)=0,\ \psi=\frac{-F}{2},\ \theta=1,\ \text{at } r=r_1\ , \tag{21}$$

$$\frac{1}{r}\frac{\partial \psi}{\partial r}=-1,\ \frac{\partial^2}{\partial r^2}\left(\frac{1}{r}\frac{\partial \psi}{\partial r}\right)=0,\ \psi=\frac{F}{2},\ \theta=0,\ \text{at } r=r_2\ . \tag{22}$$

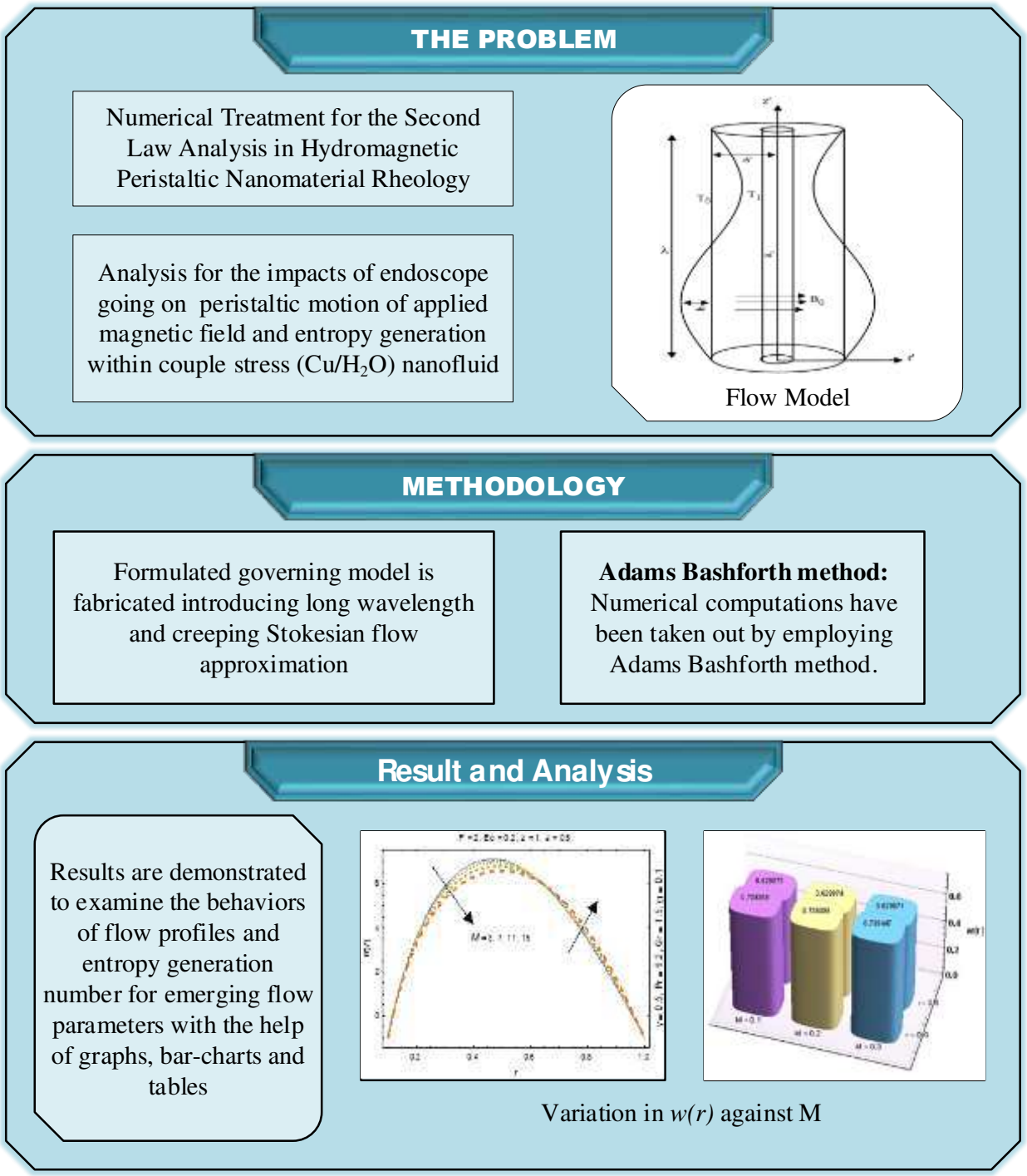

Fig. 1b: Process flow architecture

Analysis of Entropy Generation

Entropy is the measure of molecular disorder. The volumetric entropy generation rate can be expressed as [31]:

$$\dot{S}'''_{Gen} = \frac{\kappa_{nf}}{T_0^{\,2}}\left(\frac{\partial T}{\partial R}\right)^2 + \frac{\mu_{nf}}{T_0}\left(\frac{\partial W}{\partial R}\right)^2 + \frac{\sigma B_0^{\,2} W^2}{T_0}. \tag{23}$$

Moreover, characteristic entropy generation rate obtained by using boundary conditions in equation (23) is:

$$\dot{S}'''_0 = \frac{\kappa_f}{T_0^{\,2} a_2^{\,2}}\left(T_1 - T_0\right)^2, \tag{24}$$

By using equation (24) and dimensionless variables in equation (23), dimensionless entropy generation rate is:

$$N_s = \frac{\dot{S}'''_{Gen}}{\dot{S}'''_0} = A_3\left(\frac{\partial \theta}{\partial r}\right)^2 + \varepsilon Ec\,\mathrm{Pr}\,\frac{1}{A_1}\left(\frac{-1}{r^2}\frac{\partial \psi}{\partial r} + \frac{1}{r}\frac{\partial^2 \psi}{\partial r^2}\right)^2 + \varepsilon Ec\,\mathrm{Pr}\,M^2\left(\frac{1}{r}\frac{\partial \psi}{\partial r}\right)^2. \tag{25}$$

Where, $\varepsilon = \dfrac{T_0}{\left(T_1 - T_0\right)}$ represents temperature difference parameter.

Discussion of Results:

In this section, effects of important parameters on the velocity and temperature with dimensionless entropy generation number are portrayed graphically. Numerical computations have been taken out by employing Adams Bashforth method.

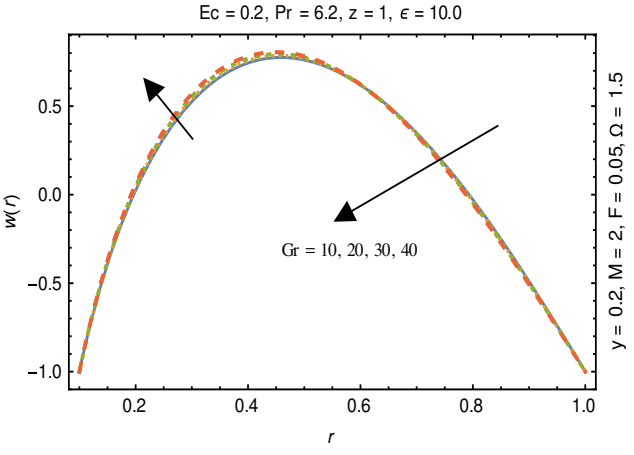

Fig. 2: Deviation in *w(r)* against G*r*.

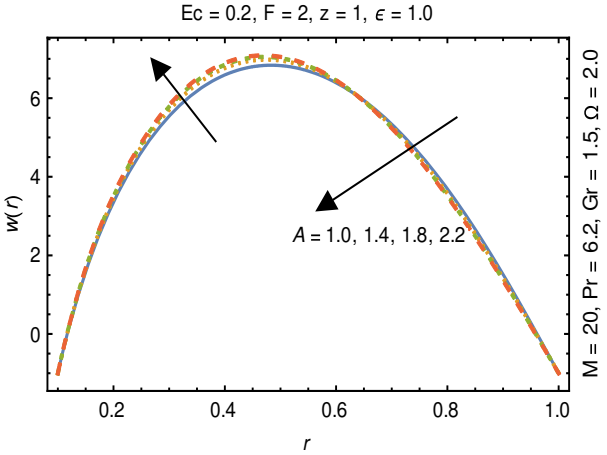

Fig. 3: Deviation of *w(r)* against y.

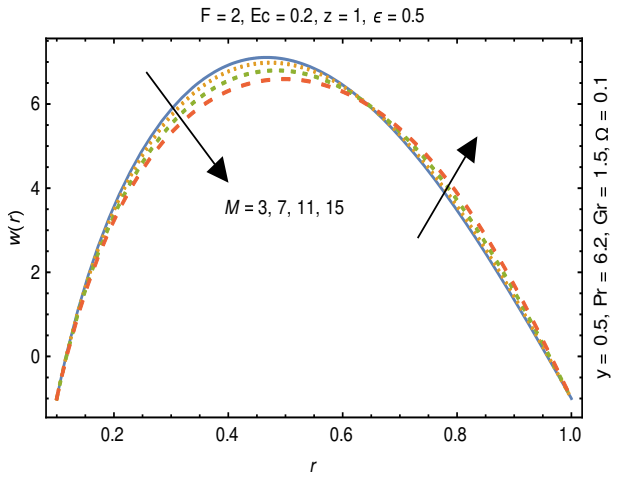

Fig. 4: Variation in *w(r)* against M.

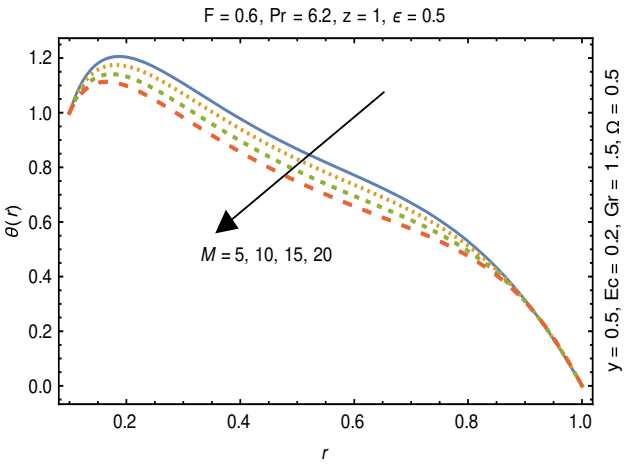

Fig. 5: Variation in $\theta(r)$ against M.

Figs. 2 and 3 portray the behavior of velocity toward rising magnitude of velocity parameter *y* and Grashof number *Gr*. It is noticed that for rising values of both parameters, *w(r)* augments close the endoscope and declines in the vicinity of the tube walls. The buoyancy forces play a leading effect close to the endoscope and hence fluid velocity upgrades as one move close to the endoscopic tube. Moreover, viscous forces are more dominant near the peristaltic tube so flow rate tends to decrease. Fig. 4 explored the oscillatory behavior of *w(r)* for several values of magnetic parameters *M*. Enlargement in velocity of the fluid near the endoscope is due to dominant effects of Lorentz force which slowly reduces near the tube wall because of no slip condition. Variational trend of temperature of the fluid is explored in Figs. 5-7. Increment in magnitude of Hartmann number causes temperature of the entire fluid to decrease as plotted in Fig. 5. Physics behind such behavior is increasing resistive effects of Lorentz force. Figs. 6 and 7 reveal that temperature increases for rising values of Ω and *Ec*. Higher values of Ω yield heat generation while increment in *Ec* leads to higher kinetic energy due to which temperature of the fluid rises. Behavior of entropy generation number *Ns* towards physical parameters is illustrated graphically and plotted in Figs. 8-11. Magnitude of entropy generation number towards *M* is increasing near the walls and in the central region including points of intersection at which entropy remains constant. This trend is due to enhancing frictional effects of Lorentz force (Fig. 8).

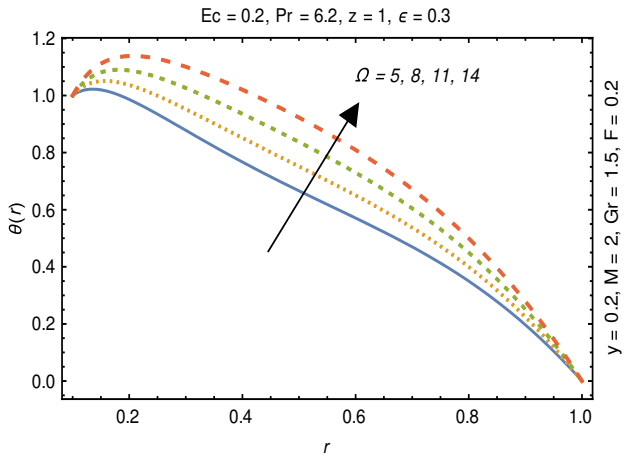

Fig. 6: Variation in $\theta(r)$ against Ω.

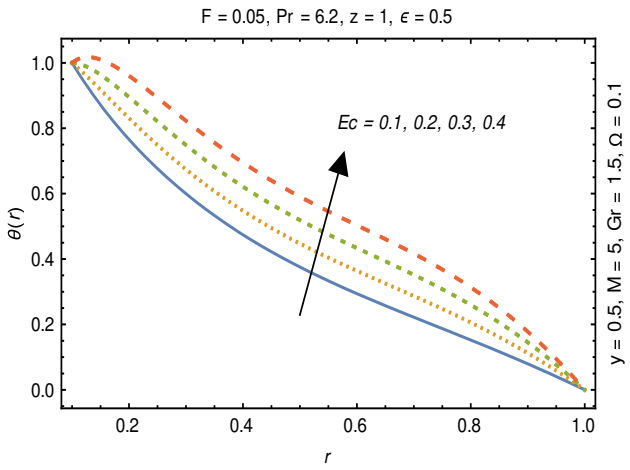

Fig. 7: Variation in $\theta(r)$ against Ec.

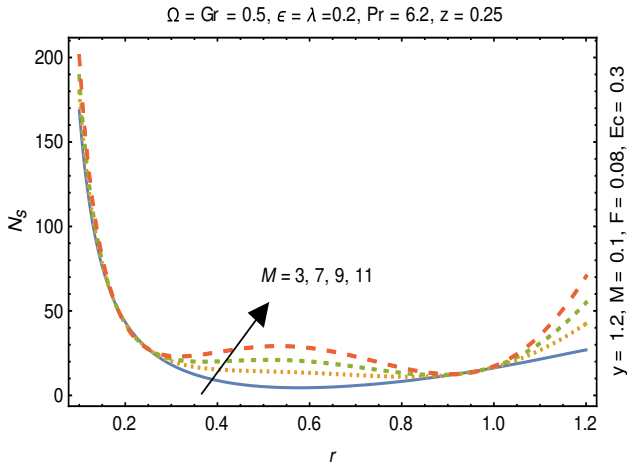

Fig. 8: Variation in N_s for M.

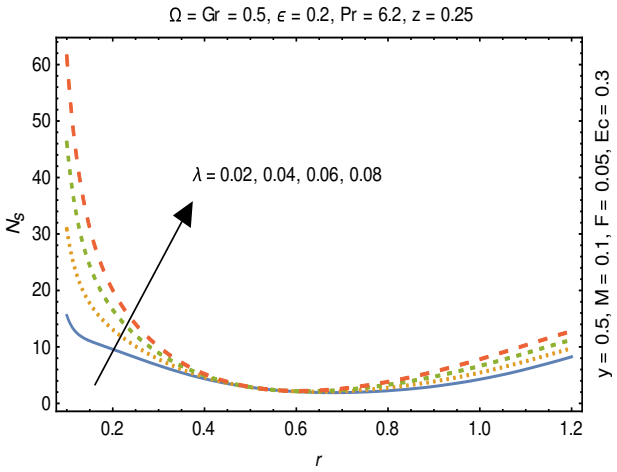

Fig. 9: Variation in N_s for λ.

Fig. 9 explicates that higher magnitude of temperature difference parameter has an impact of increasing irreversibility. Physically, it is due to high temperature gradient close to the boundaries. A similar behavior of *Ns* for *F* and *Ec* is observed from Figs. 10 and 11 that are caused by no slip wall conditions and thus large velocity gradients.

Further, numerical values for thermophysical properties of nanofluid along with empirical formulas are presented in Tables 1 and 2. Tabulated observations of velocity and temperature against rising values of nondimensional parameters are displayed in tables 3 and 4. Moreover, bar charts are drawn for a detailed view. Both of the tabulated as well as bar chart view reveal that with the variations in *Gr* and *M*, magnitude of *w(r)* increases at *r=0.4* (near endoscope) and decreases at *r=0.6* (near tube). These behaviors clearly satisfied the graphical results. Except this, *θ(r)* rises for higher magnitudes of Eckert number and Hartman number.

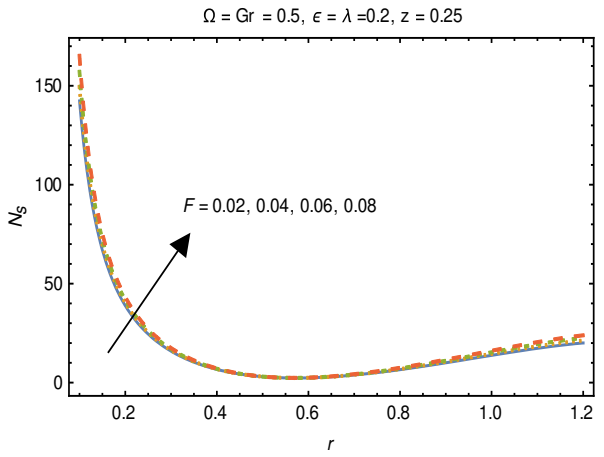

Fig. 10: Variation in N_s for F.

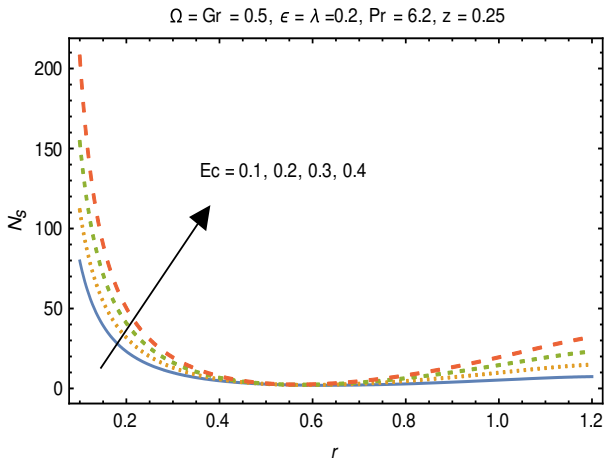

Fig. 11: Variation in N_s for *Ec*.

Table 1. Empirical values of thermophysical features for base fluid (water) and nanoparticles (Copper) [23].

Properties\ constituents	H_2O	Cu
Density, ρ(Kg/m^3)	997	8933
Specific heat, C_p (J/kg K)	4179	385
Thermal conductivity, κ (W/m K)	0.613	401
Thermal expansion coefficient, β(10^{-6}m/(mK))	210	16.65
Electrical Conductivity, σ (S/m)	0.05	5.96×10^7

Table 2. Expressions for thermophysical features for nanoparticles (Copper).

Properties	Nanofluid
Density	$\rho_{nf} = \rho_f\left[(1-\phi)+\phi\frac{\rho_s}{\rho_f}\right]$
Heat Capacity	$(\rho c_p)_{nf} = (\rho c_p)_f\left[(1-\phi)+\phi\frac{(\rho c_p)_s}{(\rho c_p)_f}\right]$
Viscosity	$\mu_{nf} = \frac{\mu_f}{(1-\phi)^{2.5}}$
Thermal conductivity	$\frac{k^*_{nf}}{k_f} = \frac{k_s+2k_f-2\phi(k_f-k_s)}{k_s+2k_f+2\phi(k_f-k_s)}$

Thermal expansion coefficient	$(\rho\beta_T)_{nf} = (\rho\beta_T)_f \left[(1\text{-}\phi) + \phi \frac{(\rho\beta_T)_s}{(\rho\beta_T)_f} \right]$
Electric conductivity	$\sigma_{nf} = \sigma_f \left[(1-\phi) + \phi \frac{\sigma_s}{\sigma_f} \right]$

Table 3. Results for velocity profile against nondimensional parameters.

Cu/H2o							
M	F	Ec	Gr	w(r=0.2)	w(r=0.4)	w(r=0.6)	w(r=0.8)
0.1	0.2	0.2	0.1	0.003951	0.739369	0.629875	-0.028079
0.2				0.003980	0.739398	0.629874	-0.028096
0.3				0.004029	0.739447	0.629871	-0.028125
	0.2			0.280305	1.21785	1.07855	0.239451
	0.4			0.648593	1.85599	1.67672	0.596190
	0.6			1.01689	2.49417	2.2749	0.952926
		0.2		0.003951	2.49425	2.27477	-0.028079
		0.4		0.003930	2.49451	2.2748	-0.028063
		0.6		0.003909	2.49477	2.27482	-0.028047
			0.1	0.002273	0.738773	0.629913	-0.021832
			0.2	0.003137	0.738816	0.62991	-0.025778
			0.3	0.004566	0.738858	0.629908	-0.029528

Table 4. Results for temperature profile against nondimensional parameters.

M	F	Ec	Gr	θ(r=0.2)	θ(r=0.4)	θ(r=0.6)
0.1	0.2	0.2	0.1	1.06589	0.544824	0.361133
0.2				1.06590	0.544827	0.361136
0.3				1.06591	0.544833	0.361142
	0.2			0.906249	1.27564	0.446693
	0.4			1.04157	1.8217	0.592958
	0.6			1.21094	2.50981	0.776021
		0.2		1.06589	0.544833	0.361142
		0.4		1.05017	0.688935	0.497805
		0.6		1.03445	0.833058	0.634488
			0.1	1.06081	0.544757	0.361070
			0.2	1.06407	0.544762	0.361075
			0.3	1.06699	0.544767	0.361079

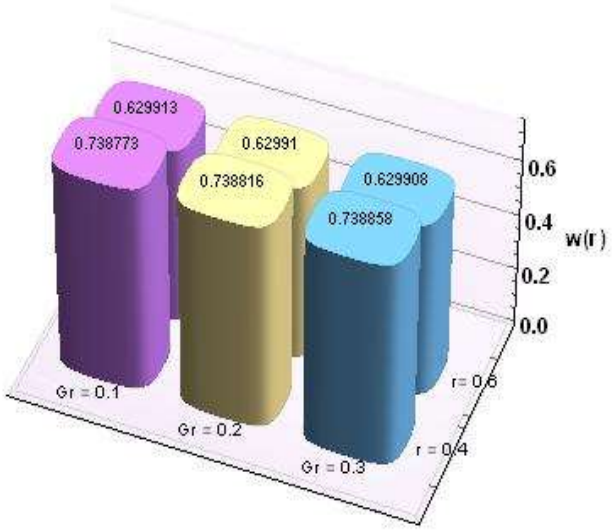

Fig. 12: Variation in *w(r)* against *Gr*.

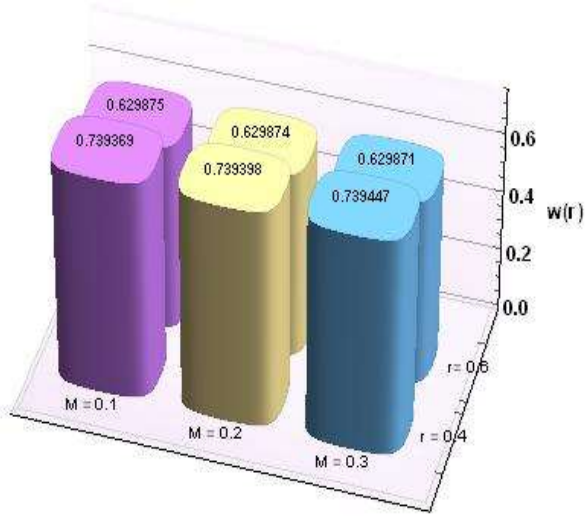

Fig. 13: Variation in *w(r)* against *M*.

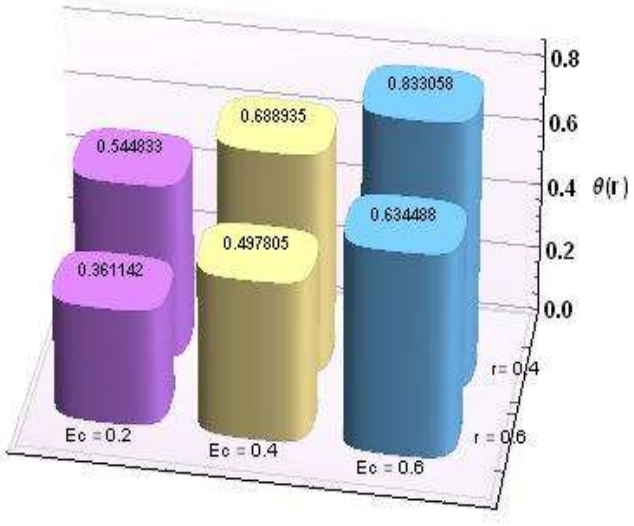

Fig. 14: Variation in *θ(r)* against *Ec*.

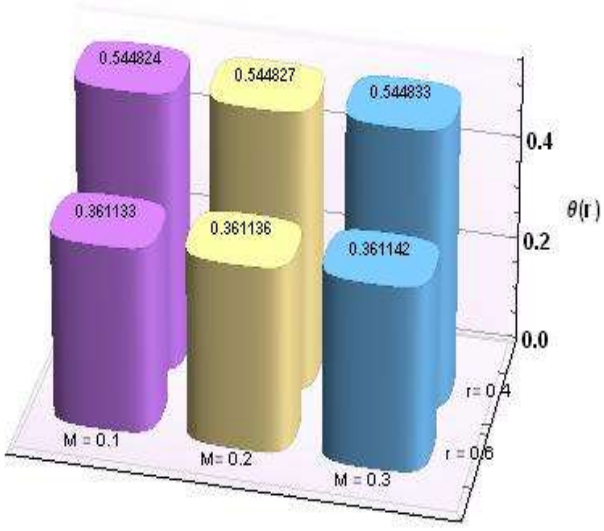

Fig. 15: Variation in *θ(r)* against *M*.

Fig. 12 and 13 are prepared to present the bar-charts showing the influence of *w(r)* against *Gr* and *M* respectively. It is observed that for radial value *r = 0.4* results are significant as compared to *r = 0.6*. Moreover Fig. 14 and 15 elucidate the effects of temperature profile *θ(r)* vs *Ec* and *M*. We noticed that temperature profile *θ(r)* signifies rapidly for larger values of Ec near the walls whereas temperature profile *θ(r)* has qualitatively similar behavior for different values of *M*.

Concluding Remarks:

In present research article, analysis for the impacts of endoscope going on peristaltic flow of couple stress nanofluid in existence of magnetic field and viscous dissipation is carried out. Major conclusions drawn from present investigation are:

- Velocity profile increases close to the endoscope and decreases close to the peristaltic vertical tube with increment of *Gr* and *y* while an opposite behavior is noticed for *M*.
- Temperature increases against higher values of Ω and *Ec* but an opposite behavior is depicted for *M*.
- Entropy is directly affected by buoyancy and viscous forces which are dominant near the endoscope and tube walls.
- The consequences of Newtonian fluid model can be obtained by taking the couple stress parameter $y = 0$ within the current model.

Future Work

In the future research, the soft computing intelligent techniques can be implemented as an efficient/accurate stochastic numerical solver implemented in nonlinear computational fluid mechanics models [33-36], singular and multi-singular differential systems [37-39] and mathematical models representing the problems of epidemiology [40-42].

Funding: None

Authors' Statements

Conceptualization: MA, MS, MAZR; **Writing Original Draft:** MA, MS, MAZR, SA, MYM, KSN; **Software:** MS, SA, MYM, KSN; **Formal Analysis:** MA, MAZR, SA; **Validation:** MYM, KSN.

References:

[1] M. Devakar and Iyengar, Run up flow of an incompressible couple stress fluid between parallel plates, Non Linear Analysis: Modeling and Control, 15 (2010) 29-37.

[2] M. Devakar D. Sreenivasu and Shankar., Analytical solutions of couple stress fluid flows with slip boundary conditions, Alexandria Engineering Journal., 53 (2014) 723–730.

[3] M. Devakar, D. Sreenivasu and Shankar, Analytical solutions of some fully developed flows of couple stress fluid between concentric cylinders with slip boundary conditions, International Journal of Engineering Mathematics., 53 (2014) 785-396.

[4] L. M. Srivastava, Flow of couple stress fluid through stenotic blood vessels, Journal of Biomechanics., 18 (1985) 479–485.

[5] D. Srinivasacharya and Srikanth, Steady streaming effect on the flow of a couple stress fluid through a constricted annulus, Archives of Mechanics., 64 (2012) 137-152.

[6] T. Hayat, M. Awais and S. A. Ambreen, Unsteady three dimensional flow of couple stress fluid over a stretching surface with chemical reaction, Nonlinear analysis: Modeling and Control., 17 (2012) 47- 59.

[7] M. Awais, S. Saleem and T. Hayat, Hydromagnetic couple-stress nanofluid flow over a moving convective wall, OHAM analysis: Acta Astronautica., 129 (2016) 271-276.

[8] D. Tripathi, R. Jhorar and OA Beg, Electro-magneto-hydrodynamic peristaltic pumping of couple stress biofluids through a complex wavy micro-channel, Journal of Modeling Liquid., 236 (2017) 358-367.

[9] J. V. R. Murthy and J. Srinivas, First and second law analysis for the MHD flow of two immiscible couple stress fluids between two parallel plates, Heat Transfer Asian Research., 43 (2014) 1–20.

[10] D. Tripathi, A. Yadav and O. A. Beg, Electro-osmotic flow of couple stress fluids in a microchannel propagated by peristalsis, European Physical Journal Plus., 132 (2017) 173-185.

[11] S. U. S. Choi and J. A. Eastman, Enhancing thermal conductivity of fluids with nano particles, in Progress of ASME, International Mechanical Engineering in Congress Exposition., 66 (1995) 99-105.

[12] S. U. Khan, S. A. Shehzad, A. Rauf and N. Ali, Mixed convection flow of couple stress nanofluid over oscillatory stretching sheet with heat absorption/generation effects, Results in Physics., 8 (2018) 1223-1231.

[13] N. A. Khan, F. Sultan, F. Riaz and M. Jamil, Investigation of combined heat and mass transfer between vertical parallel plates in a two layer flow of couple stress nanofluid, Open Engineering., 6 (2016) 35-43.

[14] H. Sithole, H. Mondal, S. Goco and P. Sibanda, Numerical simulation of couple stress nanofluid flow in magneto-porous medium with thermal radiation and a chemical reaction, Applied Mathematics and Computation., 339 (2018) 820-836.

[15] M. Tayeb, M. N. Bouaziz and S. Hanini, Influence of non-linear Boussinesq approximation and convective thermal boundary condition on MHD natural convection flow of a couple stress-nanofluid in a porous medium, Nanohybrids and Composites., 26 (2019) 45-61.

[16] N. Messaoudi, M. N. Bouaziz and H. A. Agha, Double diffusive convection in flow of couple stress nanofluid in a permeable wall of vertical channel in the presence of magnetic field, Nano Hybrids and Composites., 26 (2019) 30-44.

[17] T. W. Engelmann, Zur Physiologie des Ureter, Pflugers Archiv Gesamte Physiology., 2 (1869) 243-293.

[18] T. Hayat, H. Yasmin, B. Ahmad and B. Chen, Simultaneous effects of convective conditions and nanoparticles on the peristaltic motion, Journal of Molecular Liquids., 193 (2014) 74-82.

[19] K. Vajravelu, G. Radhakrishnamacharya and Radhakrishnamurty, Peristaltic flow and heat transfer in a vertical porous annulus with long wave approximation, International Journal of Non-Linear Mechanics., 42 (2007) 754–759.

[20] I. Shahzadi and Nadeem, Inclined magnetic field analysis for metallic nanoparticles submerged in blood with convective boundary condition, Journal of Molecular Liquids., 230 (2017) 61–73.

[21] T. Hayat, M. Rafiq, B. Ahmad, and S. Asghar, Entropy generation analysis for peristaltic flow of nanoparticles in a rotating frame, International Journal of Heat and Mass Transfer., 108 (2017) 1775–1786.

[22] S. Jangili, S. O. Adesanya, H. A. Ogunseye and R. Lebelo, Couple stress fluid flow with variable properties: a second law analysis., Mathematical Methods Applied Science., 42 (2019) 85–98.

[23] M. A. Abbas, Y. Bai, M. M. Rashidi and M. M. Bhatti, Analysis of entropy generation in the flow of peristaltic nanofluid in channel with complaint walls, Entropy., 18 (2016) 18030090.

[24] F. M. Abbasi, Shanakhat and Shehzad, Entropy generation analysis for peristalsis of nanofluid with temperature dependent viscosity and Hall effects, Journal of Magnetic Matter., 474 (2019) 434–441.

[25] M. Ali, W. A. Khan, M. Irfan, F. Sultan, M. Shahzad and M. Khan, Computational analysis of entropy generation for cross-nanofluid flow, Applied Nanoscience., 48 (2019) 1–11.

[26] S. E. Awan, Z. A. Khan, M. Awais, S. U. Rehman and M. A. Z. Raja, Numerical treatment for hydro-magnetic unsteady channel flow of nanofluid with heat transfer, Results in Physics., 9 (2018) 1543-1554.
[27] M. Nawaz, S. Rana and I. H. Qureshi, Computational fluid dynamics simulations for dispersion of nanoparticles in a magnetohydrodynamic liquid: a Galerkin finite element method, RSC Advances., 8 (2018) 38324-38335.

[28] M. A. Abbas, Y. Bai, M. M. Rashidi and M. M. Bhatti, Application of drug delivery in megnetohydrodynamics peristaltic blood flow of nano fluid in a non-uniform channel, Journal of Mechanics in Medicine and Biology., 16 (2016) 1650052.
[29] P. Rana and N. Shukla, Entropy generation analysis for non-similar analytical study of nanofluid flow and heat transfer under the influence of aligned magnetic field, Alexandria Engineering Journal., 57 (2018) 3299-3310.
[30] Alkanhal, M. Sheikholeslami, A. Arabkoohsar, R. Haq, A. Shafee, Z. Lif and I. Tlili, Simulation of convection heat transfer of magnetic nanoparticles including entropy generation using CVFEM, International Journal of Heat Mass Transfer., 136 (2019), 146–156.
[31] N. S. Akbar, M. Raza and R. Ellahi, Endoscopic effects with entropy generation analysis in peristalsis for the thermal conductivity of copper-water nanofluid, Journal of Applied Fluid Mechanics, 9 (2016) 1721-1730.
[32] K. Rameesh and M. Devakar, Effect of endoscope on the peristaltic transport of a couple stress fluid with heat transfer: Application to biomedicine, Nonlinear Engineering., 8 (2019) 619-629.
[33] Ilyas, H., et al., 2021. A novel design of Gaussian Wavelet Neural Networks for nonlinear Falkner-Skan systems in fluid dynamics. Chinese Journal of Physics.
[34] Shoaib, M., et al., 2021. Neuro-Computing Networks for Entropy Generation under the Influence of MHD and Thermal Radiation. Surfaces and Interfaces, p.101243.
[35] Aljohani, J.L., et al., 2021. Intelligent computing through neural networks for numerical treatment of non-Newtonian wire coating analysis model. Scientific Reports, 11(1), pp.1-32.
[36] Uddin, I., et al., 2021. Design of intelligent computing networks for numerical treatment of thin film flow of Maxwell nanofluid over a stretched and rotating surface. Surfaces and Interfaces, p.101107.

[37] Sabir, Z., et al., 2021. A novel design of fractional Mayer wavelet neural networks with application to the nonlinear singular fractional Lane-Emden systems. Alexandria Engineering Journal, 60 (2), 2641-2659.
[38] Sabir, Z., et al., A neuro-swarming intelligence based computing for second order singular periodic nonlinear boundary value problems.
[39] Sabir, Z., et al., 2020. Design of stochastic numerical solver for the solution of singular three-point second-order boundary value problems. Neural Computing and Applications, pp.1-17.
[40] Ahmad, I., et al., 2019. Novel applications of intelligent computing paradigms for the analysis of nonlinear reactive transport model of the fluid in soft tissues and microvessels. Neural Computing and Applications, 31(12), pp.9041-9059.
[41] Ahmad, I., et al., 2020. Integrated neuro-evolution-based computing solver for dynamics of nonlinear corneal shape model numerically. Neural Computing and Applications, pp.1-17.
[42] Shoaib, M., et al., 2021. A Stochastic Numerical Analysis Based on Hybrid NAR-RBFs Networks Nonlinear SITR Model for Novel COVID-19 Dynamics. Computer Methods and Programs in Biomedicine, p.105973.